

**Photovoltaic performance and characteristics of dye sensitized solar cells prepared with the N719 thermal degradation products [Ru(L-H)<sub>2</sub>(NCS)(4-tert-butylpyridine)]-, +N(Bu)<sub>4</sub> and [Ru(L-H)<sub>2</sub>(NCS)(1-methylbenzimidazole)]-, +N(Bu)<sub>4</sub>**

Phuong, Nguyen Tuyet; Xuan Thi Lam, Binh ; Hansen, Poul Erik; Lund, Torben; Andersen, Anders Rand

*Published in:*  
European Journal of Inorganic Chemistry

*DOI:*  
[10.1002/ejic.201000935](https://doi.org/10.1002/ejic.201000935)

*Publication date:*  
2011

*Document Version*  
Early version, also known as pre-print

*Citation for published version (APA):*

Phuong, N. T., Xuan Thi Lam, B., Hansen, P. E., Lund, T., & Andersen, A. R. (2011). Photovoltaic performance and characteristics of dye sensitized solar cells prepared with the N719 thermal degradation products [Ru(L-H)<sub>2</sub>(NCS)(4-tert-butylpyridine)]-, +N(Bu)<sub>4</sub> and [Ru(L-H)<sub>2</sub>(NCS)(1-methylbenzimidazole)]-, +N(Bu)<sub>4</sub>. *European Journal of Inorganic Chemistry*, 2011(16), 2533-2539. <https://doi.org/10.1002/ejic.201000935>

**General rights**

Copyright and moral rights for the publications made accessible in the public portal are retained by the authors and/or other copyright owners and it is a condition of accessing publications that users recognise and abide by the legal requirements associated with these rights.

- Users may download and print one copy of any publication from the public portal for the purpose of private study or research.
- You may not further distribute the material or use it for any profit-making activity or commercial gain.
- You may freely distribute the URL identifying the publication in the public portal.

**Take down policy**

If you believe that this document breaches copyright please contact [rucforsk@kb.dk](mailto:rucforsk@kb.dk) providing details, and we will remove access to the work immediately and investigate your claim.

# Photovoltaic Performance and Characteristics of Dye-Sensitized Solar Cells Prepared with the N719 Thermal Degradation Products [Ru(LH)<sub>2</sub>(NCS)(4-*tert*-butylpyridine)][N(Bu)<sub>4</sub>] and [Ru(LH)<sub>2</sub>(NCS)(1-methylbenzimidazole)][N(Bu)<sub>4</sub>]

Phuong Tuyet Nguyen,<sup>[a]</sup> Binh Xuan Thi Lam,<sup>[a]</sup> Anders Rand Andersen,<sup>[b,c]</sup>  
Poul Erik Hansen,<sup>[a]</sup> and Torben Lund\*<sup>[a]</sup>

**Keywords:** Solar cells / Dyes / Electrochemistry / Sensitizers

The dye-sensitized solar cell N719 thermal degradation products [Ru(LH)<sub>2</sub>(NCS)(4-*tert*-butylpyridine)][N(Bu)<sub>4</sub>] (**1**) and [Ru(LH)<sub>2</sub>(NCS)(1-methylbenzimidazole)][N(Bu)<sub>4</sub>] (**2**) were synthesized from [Ru(LH)<sub>2</sub>(NCS)<sub>2</sub>][N(Bu)<sub>4</sub>]<sub>2</sub> (N719), (LH = 2,2'-bipyridyl-4,4'-dicarboxylic acid) and characterized by electrospray mass spectrometry and NMR spectroscopy. Dye-sensitized solar cells (DSCs or DSSCs) prepared with **1** and **2** have efficiencies that are three and two times lower than N719 cells, respectively. Analysis of the UV/Vis and incident-photon-to-current efficiency (IPCE) spectra indicates that the main reason for the reduced efficiencies is a reduced electron collection efficiency ( $\eta_{\text{coll}}$ ). The substituted dyes give rise to lower potentials and currents. When measured at open circuit voltage illumination, the impedance is very different for

such cells relative to N719 cells. Furthermore, the lifetime ( $\tau_{\text{eff}}$ ) of the electrons in the TiO<sub>2</sub> is reduced by a factor of around ten. The low  $\tau_{\text{eff}}$  values may be related to the positive charge on dyes **1** and **2**, which results in an enhanced local concentration of I<sub>3</sub><sup>−</sup> near the photoanode and thereby a higher dark current. N719 cells at higher temperature result in slightly lower potentials, and this alone leads to a change in impedance response when measured at open circuit voltage. The same parts of the impedance spectrum are affected (i.e., the interface between the photoanode and the electrolyte is affected in the same way) when we compare data from N719 heated cells and DSCs prepared with **1** or **2** and not thermally treated.

## Introduction

Dye-sensitized solar cells (DSC) have received widespread interest due to their potential as low-cost photovoltaics.<sup>[1–8]</sup> DSCs with areas less than 1.3 cm<sup>2</sup> have been prepared with efficiencies of 7–8% by using the ruthenium dye N719 as sensitizer and an electrolyte mixture that comprises LiI (0.1 M), hexylmethylimidazolium iodide (0.6 M), I<sub>2</sub> (0.05 M), and high concentrations of the additive 4-*tert*-butylpyridine (4-TBP) or 1-methylbenzimidazole (MBI) dissolved in acetonitrile<sup>[9]</sup> (see Figure 1).

4-TBP and MBI as electrolyte additives increase the  $V_{\text{oc}}$  of the DSC by 200–300 mV and the overall efficiency of the DSC by 1–2%.<sup>[10–12]</sup> Whereas these additives have a very positive effect on the efficiency of the cell, they cause problems with thiocyanate-containing sensitizers in terms of thiocyanate substitution reactions at elevated temperatures.

[a] Department of Science, Systems and Models, Roskilde University, Universitetsvej 1, 4000 Roskilde, Denmark  
Fax: +45-46743011  
E-mail: tlund@ruc.dk

[b] University of Southern Denmark, Institute of Sensors, Signals and Electrotechnics (SENSE), Niels Bohrs Allé 1, 5230 Odense M, Denmark

[c] Danish Technological Institute, Plastics Technology, Gregersensvej 2630 Taastrup, Denmark

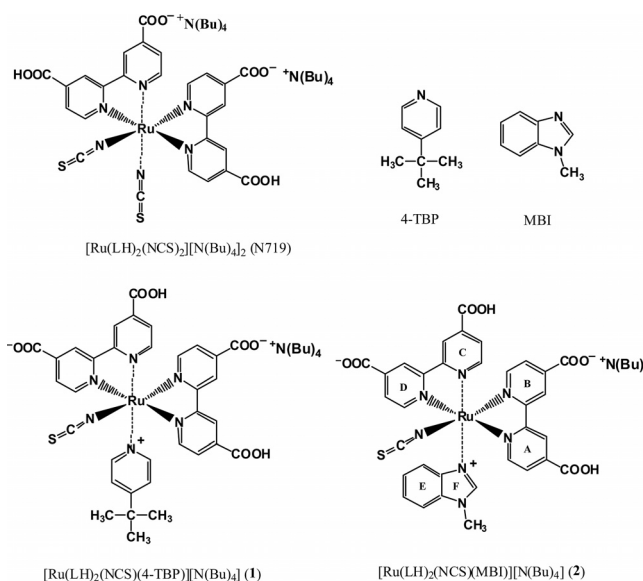
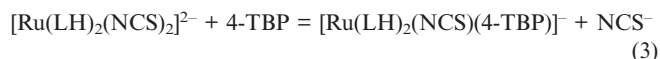
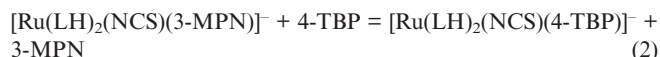
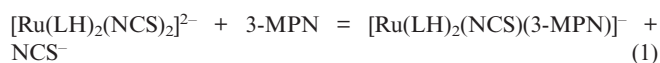


Figure 1. Structures of ruthenium dye N719, DSC electrolyte additives 4-TBP and MBI, and additive substitution products **1** and **2**; LH<sub>2</sub> = 2,2'-bipyridyl-4,4'-dicarboxylic acid.

We have recently shown that ruthenium dyes N719 and Z907 may undergo ligand-substitution reactions with 3-

methoxypropionitrile (3-MPN) and 4-TBP at elevated temperatures ( $> 80\text{ }^{\circ}\text{C}$ ) according to the mechanism shown in Equations (1), (2), and (3).<sup>[13–15]</sup>



The half-life of the N719 dye at  $85\text{ }^{\circ}\text{C}$  in DSCs prepared with an electrolyte that contains 4-TBP is 120 h, which is far less than that required to fulfill the 1000 h standard thermal/light-soaking stress test at  $85\text{ }^{\circ}\text{C}$ .<sup>[16]</sup> The MBI additive reacts with N719 by a similar mechanism with a half-life of about 300 h.<sup>[17]</sup>

The thermal degradation products of N719,  $[\text{Ru}(\text{LH})_2(\text{NCS})(4\text{-TBP})]^{-}$ , and  $[\text{Ru}(\text{LH})_2(\text{NCS})(\text{MBI})]^{-}$ , are themselves sensitizers, and it may therefore be argued that transformation of the N719 dye to  $[\text{Ru}(\text{LH})_2(\text{NCS})(\text{additive})]^{-}$  may only have a minor influence on the DSC performance.

In this work we compare the photovoltaic performance and characteristics of DSCs prepared with the substitution products **1** and **2** to those of N719. These cells are referred to as DSCN719, DSC1 and DSC2 in the following discussion. The substitution products were synthesized, characterized, and applied as dyes in DSCs, and their performance characteristics were tested by using current–voltage ( $J$ – $V$ ) curves and incident-photon-to-current efficiency (IPCE) measurements. Furthermore, electrochemical impedance spectroscopy (EIS) was applied to DSC1 and **2**, and the results were compared with similar data obtained in a similar manner for freshly prepared and thermally aged DSCN719.

## Results and Discussion

### Synthesis of **1** and **2**

Products **1** and **2** (Figure 1) were synthesized by heating N719 with either 4-TBP or MBI in dimethylformamide (DMF) at  $120\text{ }^{\circ}\text{C}$  for 48 h. DMF was chosen as solvent, because it does not react with N719 by thiocyanate ligand substitution like 3-methoxypropionitrile. Products **1** and **2** were purified by using a strong cation-exchange column and by taking advantage of the fact that the charges of the complexes are +1 at low pH. Minor amounts of unreacted N719, DMF, and other neutral impurities were removed by the ion-exchange purification. As shown in Figure 2, the chromatogram from LC–UV/Vis–MS analysis of the purified product of the reaction between N719 and MBI only contains one peak at a retention time ( $t_R$ ) of 24 min. The peak may be identified as fully protonated product  $[\text{RuL}_2(\text{NCS})(\text{MBI})]^+$  (**2**) (DSC2) on the basis of an absorption maximum at  $\lambda = 518\text{ nm}$  and a molecular ion  $[\text{M}]^+$

value of  $m/z = 780$ . The identification is furthermore supported by a fragmentation of the MBI ligand by  $\text{MS}^2$ :  $m/z = 780 \rightarrow m/z = 648$ , which is similar to the fragmentation previously reported for complex **1**.<sup>[15]</sup>

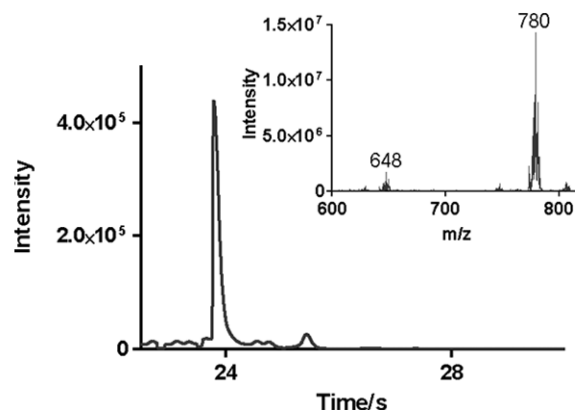


Figure 2. LC–UV/Vis chromatogram obtained at  $\lambda_{\text{max}}$  in the interval 400–800 nm of a sample of the purified fully protonated substitution product **2**. The inset shows an electrospray mass spectrum of the fully protonated compound  $[\text{RuL}_2(\text{NCS})(\text{MBI})]^+$  (**2**).

### NMR Spectroscopic Characterization of **2**

The  $^1\text{H}$  and  $^{13}\text{C}$  NMR spectra of **2** show no sign of symmetry. Furthermore, both in  $\text{D}_2\text{O}$  and in a  $\text{D}_2\text{O}/[\text{D}_6]\text{DMF}$  (1:1) mixture, a number of resonances are broad. Both solutions were made basic with NaOH to increase the solubility. Cooling of the solutions to  $5\text{ }^{\circ}\text{C}$  led to new resonances both in  $\text{D}_2\text{O}$  and in a  $\text{D}_2\text{O}/[\text{D}_6]\text{DMF}$  (1:1), but the new resonances were less intense than the original ones.

The  $^1\text{H}$  NMR spectra in  $\text{D}_2\text{O}$  are very complex, and most of the resonances are broad. The discussion will therefore concentrate on the spectra in  $\text{D}_2\text{O}/[\text{D}_6]\text{DMF}$  (1:1) (Figure 3). In the  $^1\text{H}$  NMR spectra at  $25\text{ }^{\circ}\text{C}$  shown in Figure 3a, the H-5 resonances are sharp, and so are those from the 1-methylimidazole moiety, with the exception of H-2. The H-3 protons are divided into two groups. Two are sharp and two are broad, whereas all H-6 protons are broad at 600 MHz but sharper and show splittings due to couplings at 300 MHz. H-2F and H-4E are also broad. The H-6 protons have rather different  $^1\text{H}$  chemical shifts (see Figure 3a). Upon cooling to  $5\text{ }^{\circ}\text{C}$ , three of the four H-6 resonances and the H-2 resonance split into two at 600 MHz. A similar effect can be seen at 300 MHz at  $-20\text{ }^{\circ}\text{C}$  (Figure 3b).

The  $^{13}\text{C}$  NMR spectrum shows separate signals for all carbon atoms, but some signals are broad. As the solubility of the compound is limited, it was not possible to obtain a  $^{13}\text{C}$  NMR spectrum at low temperature. The broad resonances are ascribed to resonances that come from C-6-type carbon atoms. The  $^{13}\text{C}$  NMR chemical shift of the NCS group is at  $\delta = 137.0\text{ ppm}$ , which shows that this is coordinated to the nitrogen.<sup>[18]</sup> Complex **2**, which has only one NCS ligand, provides a possibility for testing the hypothesis by Shklover et al. that the proton chemical shifts of the

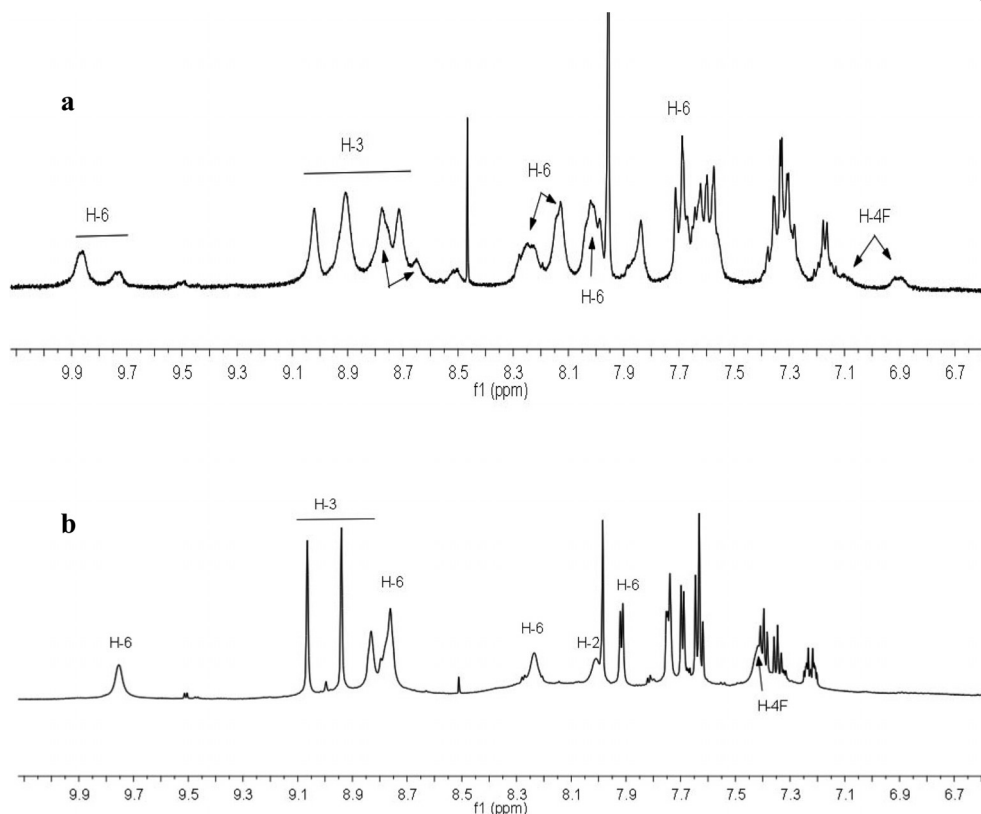


Figure 3. (a) 600 MHz  $^1\text{H}$  NMR spectrum of the aromatic region of **2** at 25 °C in  $\text{D}_2\text{O}/\text{DMF}$  (1:1). (b) 300 MHz  $^1\text{H}$  NMR spectrum of the same region but at  $-20^\circ\text{C}$ .

pyridine ring *trans* to the NCS ligand are the ones at low field.<sup>[18]</sup> From the  $^{13}\text{C}$  NMR spectrum, it can be determined that all four C-4 carbon atoms are rather close in chemical shift, and so are those of C-3, C-5, and possibly also C-2 and C-6. In other words, *trans* coordination does not lead to any dramatic influence on  $^{13}\text{C}$  NMR chemical shifts.

In the  $^1\text{H}$  NMR spectrum, the rather low-field shift of the H-3 protons can be explained by mutual polarization as, for example, observed for the H-4 and H-5 protons of phenanthrene.<sup>[19]</sup> For H-6, the two high-field positions in N719 may be caused by ring currents. In **2**, the third H-6 proton is also shifted to high field, as this is now positioned above the face of the MBI rings. NCS may play a general role but, according to our results, not a stereospecific one.

### Structural Implications

The  $^1\text{H}$  NMR chemical shifts of **2** are to a large extent similar to those of N719.<sup>[18]</sup> The main difference is the shift of one of the H-6 protons, which is shifted to high field by approximately 1 ppm in **2**. This can best be explained by the new position of this proton above the surface of the MBI rings, subjecting it to a high-field shift. The broadness of the H-6 protons, two of the H-3 protons, and the H-2(F) and H-4(F) protons at 600 MHz suggests a structural averaging. The finding of two sets of resonances at lower temperature suggests two different forms as shown in Figure 4. The A form seems to be the most stable as judged

from the H-2(F) and H-4(F) chemical shifts. The slight differences in the H-6 chemical shifts of the two forms, despite the fact that the H-6C proton is not close to the MBI rings, can be explained by the slight variation in positions of the bipyridyl rings in the two forms, which leads to different ring current effects.

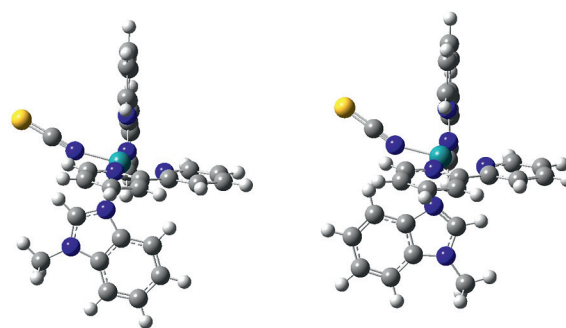


Figure 4. Two different forms of **2** calculated with the Gaussian 09 package.

### Calculations

Structures are calculated with the Gaussian 09 package.<sup>[23]</sup> Hartree–Fock (HF) type calculations were carried out with a STO-3G(d,p) basis set. The obtained structures are rather similar to the X-ray structure for the tetraester of N719.<sup>[16]</sup> The two structures in Figure 4 are very similar

with respect to the  $[\text{Ru}(\text{LH})_2(\text{NCS})]$  part. Only the MBI molecule has two different orientations. This leads to some minor distance changes in the  $[\text{Ru}(\text{LH})_2(\text{NCS})]$  part.

### The Performance of **1** and **2** as Sensitizers

Figure 5 shows the UV/Vis spectra of the two additive substitution products **1** and **2** obtained in ethanol together with the spectrum of N719.

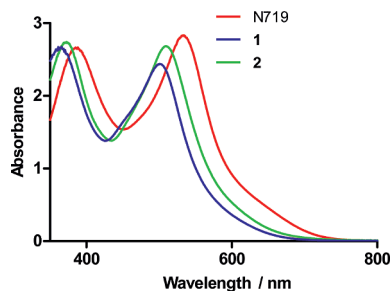


Figure 5. UV/Vis spectra of N719, **1**, and **2** obtained in ethanol. The absorption maxima of the three compounds are 535, 503, and 510 nm, respectively.

As shown in Figure 5, the spectra of **1** and **2** are blue-shifted by 32 and 25 nm relative to N719. The blue-shifts of **1** and **2** would reduce the efficiencies of the two cells relative to a N719 cell by around 25% and around 15%, in that order, assuming that all other parameters of the three cells were identical and an AM1.5 light intensity distribution.

Figure 6 shows incident-photon-to-current efficiency [IPCE( $\lambda$ )] curves of DSCs prepared with N719, **1**, or **2** with MBI as electrolyte additive.

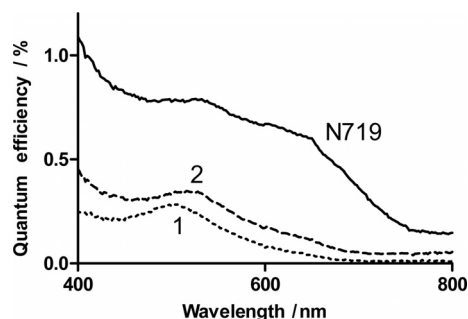


Figure 6. DSCs prepared with N719, **1**, and **2** as sensitizers with MBI as additive. The IPCE measurements are not corrected for light reflections.

Figure 6 shows that the IPCE of DSC1 and DSC2 are reduced relative to that of DSCN719. The maximum quantum yields of the three dyes **1**, **2**, and N719 at their respective absorption maxima are 0.27, 0.32, and 0.80. The reduction in  $\text{IPCE}(\lambda) = \text{LHE}(\lambda) \phi_{\text{inj}} \eta_{\text{coll}}$  (for which  $\phi_{\text{inj}}$  and  $\eta_{\text{coll}}$  are the injection and electron collection efficiencies, respectively) cannot be explained by differences in the light absorption harvesting efficiencies  $[\text{LHE}(\lambda)]$  of the three dyes, and the differences have to be attributed to a reduced value of  $\phi_{\text{inj}} \eta_{\text{coll}}$ .<sup>[2]</sup> The  $\eta_{\text{inj}}$  is likely to be close to around 1

for all the three dyes, and  $\eta_{\text{coll}}$  may therefore be identified as the main parameter responsible for the reduction in the IPCE values of DSC1 and DSC2.

The  $J$ - $V$  curves of DSCs N719, **1**, and **2** with 4-TBP and MBI as additives were obtained at a light intensity of  $100 \text{ W m}^{-2}$  from a Xenon light source with a spectral distribution close to that of the AM1.5 standard. The  $J$ - $V$  curves with MBI as additive are shown in Figure 7, and the efficiencies of the cells are shown in Figure 8. All the performance data (energy conversion efficiency,  $\eta$ , short current,  $I_{\text{sh}}$ , open circuit voltage,  $V_{\text{oc}}$ , and fill factor, FF) are shown in Table 1.

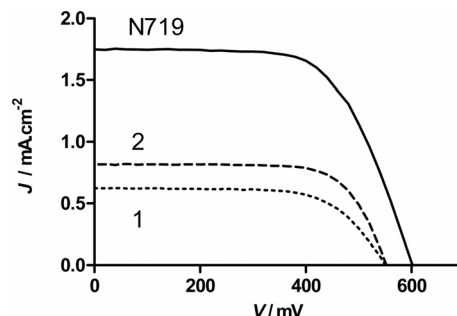


Figure 7. The  $J$ - $V$  curves of DSCs prepared with N719, **1**, and **2** as sensitizers and MBI as additive obtained at  $100 \text{ W m}^{-2}$ .

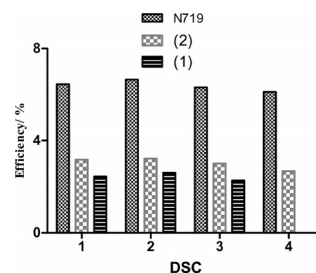


Figure 8. Efficiencies of four sets of DSCs prepared with N719, **1**, and **2** as dyes and MBI as additive.

Table 1. DSC performance data obtained at  $100 \text{ W m}^{-2}$ .<sup>[a,b]</sup> The DSCs were prepared with N719, **1**, and **2** as sensitizers, and MBI and 4-TBP as additives.

Additive	$I_{\text{sh}}$ [mA]	$V_{\text{oc}}$ [mV]	FF	$\eta$ [%]
N719	15.68	631.61	0.64	7.05
<b>2</b> MBI	6.96	553.82	0.72	3.23
<b>1</b>	6.26	543.94	0.66	2.61
N719	13.62	595.96	0.59	6.20
<b>2</b> 4-TBP	6.48	555.03	0.70	3.07
<b>1</b>	6.67	535.49	0.63	2.77

[a] Cell areas:  $8 \text{ cm}^2$ . [b] Average values for three cells.

As shown in Figure 8 and Table 1, the efficiencies of DSC1 and DSC2 are reduced by a factor of three and two, respectively, relative to DSCN719. The reduced efficiency of DSC1 and DSC2 is mainly related to reduction of the short current,  $I_{\text{sh}}$ , which is closely linked to the IPCE. The observation of nearly the same reduction of the  $I_{\text{sh}}$  and IPCE values of **1** and **2** relative to N719 (by a factor of 2–3) is therefore not surprising.



### Electrochemical Impedance Spectroscopy

EIS analysis was performed on DSCN719, DSC1, and DSC2 with MBI and 4-TBP as additives. Normal cells prepared with N719 were heated at 85 °C for 20 and 140 h, and they were characterized before and after heating. Representative Bode and Nyquist plots are shown in Figures 9 and 10. For details on the interpretation of solar cell impedance data, see ref.<sup>[20]</sup>

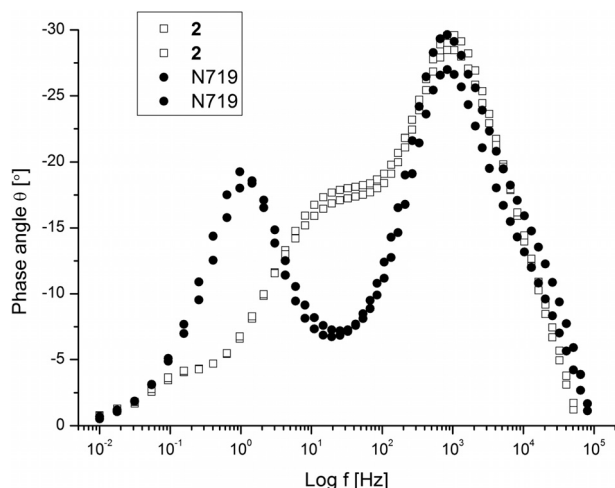


Figure 9. Phase angle vs. frequency for two cells of DSCN719 (black circles) and two cells of DSC2 (squares). EIS data were obtained under illumination. All cells contained MBI as additive.

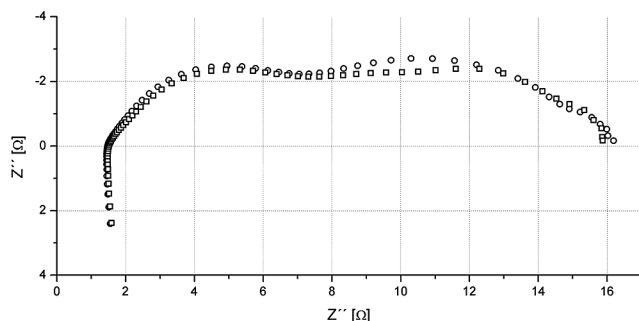


Figure 10. Nyquist plot showing data from two cells of DSC2 with MBI as additive. The positive values in  $Z'$  are the highest frequency data and show the effect of contacts and leads. The two main arcs (counter-electrode arc at highest frequency and photoelectrode arc at middle frequency) overlap, and detailed analysis is somewhat difficult.

The impedance shows the same general feature for both cells DSC1 and DSC2, no matter what additive was used. Examples of these curves are shown in Figures 9 and 10. Figure 9 shows the phase part of the impedance as a function of frequency for cells DSCN719 and DSC2. A DSC phase plot (Bode type plot) obtained at moderate potentials will usually contain three peaks. In the kHz region, we see a peak that is associated with the charge transfer at the counter-electrode, and in the 1–10 Hz region, the peak corresponds to the photoelectrode impedance. The latter impedance is not a simple charge-transfer process but can be modeled by an electric transmission line (TL) model.<sup>[20]</sup> In

the mHz region, one sometimes observes a peak that is associated with ionic diffusion in the electrolyte, but in most cases the impedance data obtained in this work do not show any clear features of this kind. Similarly, a Nyquist plot representation will show three more or less pronounced arcs that correspond to the above-mentioned processes. The Nyquist plot (Figure 10) is difficult to interpret because of the very dominating counter-electrode (CE) arc at the high frequencies. The big CE arc is caused by voltage loss in the glass substrate. Pilkington K-glass is not optimized for DSC purposes and it has a high sheet resistance.

On average, DSC1 cells reached 0.514 V with 4-TBP as additive, but only 0.491 V with MBI as additives, whereas DSC2 cells reached 0.544 V and 0.548 V with the same additives as used for DSC1. In comparison, DSCN719 cells were able to reach slightly higher potentials at 0.562 V and 0.596 V.

One way of illustrating the consequence of the lower potentials caused by degraded dyes is to calculate the electron lifetime  $\tau_{\text{eff}}$  for the  $\text{TiO}_2$  photoelectrode part of the cell.

From the Bode plots, the electron lifetimes were obtained for DSCs prepared with 1, 2, and N719. An estimated value for electron lifetime in the photoelectrode,  $\tau_{\text{eff}} = R_{\text{rec}} C_{\text{PE}}$ , for which  $R_{\text{rec}}$  is the resistance towards recombination and  $C_{\text{PE}}$  is the capacitance of the  $\text{TiO}_2$ /electrolyte interface, can be derived from the Bode plot by using Equation (4).

$$\tau_{\text{eff}} = \frac{1}{2\pi f_{\text{min}}} \quad (4)$$

The  $f_{\text{min}}$  value is read off the Bode plot at the phase angle peak observed around 1–10 Hz. The N719 cells were also characterized after 20 and 140 h in the dark at 85 °C. The electron lifetimes  $\tau_{\text{eff}}$  are shown in Table 2.

Table 2. Electron lifetimes of the injected electrons in the  $\text{TiO}_2$  conduction band of DSC1, DSC2 and DSCN719 cells stored between 0–140 h in dark at 85 °C.<sup>[a,b]</sup>

Dye	Additive <sup>[c]</sup>	Heating time [h] at 85 °C	$\tau_{\text{eff}}$ [s]
N719	4-TBP	0	0.168
N719	MBI	0	0.188
N719	No additive	0	0.159
1	4-TBP	0	0.032
1	MBI	0	0.020
2	4-TBP	0	0.053
2	MBI	0	0.015
N719	4-TBP	20	0.024
N719	MBI	20	0.130
N719	No additive	20	0.052
N719	4-TBP	140	0.005
N719	MBI	140	0.011
N719	No additive	140	0.002

[a] The  $\tau_{\text{eff}}$  values were read off from the Bode plots in Figure 10.

[b] The lifetimes are average values obtained from at least two cells.

[c] [additive] = 0.5 M.

The electron lifetimes for cells with N719 that have been heated at 85 °C resemble those measured in DSC1 or DSC2. The EIS analysis could therefore suggest that the

some of the drop in the electron lifetime in the thermally treated DSCs is caused by the formation of the N719 substitution products **1** and **2**, which is in agreement with our previous conclusions based on HPLC product analysis of thermally treated cells.<sup>[13–15]</sup> A much more detailed account of the determinations and analysis of the electron lifetime  $\tau_{\text{eff}}$  in  $\text{TiO}_2$  will be given elsewhere.<sup>[21]</sup>

One observation that may explain some of the reduced performance of the heated cells DSCN719 and the cells DSC1 and DSC2 is that these cells, according to our investigations, share the same electric characteristics of the photo-electrode–electrolyte interface. By the thermal treatment of DSCN719, or equivalently, by preparing the cells with the substitution products **1** or **2**, the charge of the interface becomes more positive relative to the N719-dyed interphase. A positive charge located on the nitrogen atoms of the pyridine or benzimidazole ligands of the substituted dye attached to the  $\text{TiO}_2$  surface will reverse the charge distribution of the photoanode double layer and thereby facilitate the incorporation of  $\text{I}_3^-$  into the double layer structure. A higher outer-surface concentration of  $\text{I}_3^-$  in close vicinity to the electrode would then electrostatically enhance the dark current and lower the potential, and thereby reduce the electron lifetime to a lower value than would otherwise be observed for a more neutral interface.<sup>[22]</sup> However, the iodide chemistry at the interface seems to be rather complex, and hence further details in relation to this approach will be shown elsewhere in a detailed impedance experiment, which is currently being worked out.<sup>[21]</sup>

## Conclusions

DSCs prepared with the two N719 thermal additive substitution products,  $[\text{Ru}(\text{LH})_2(\text{NCS})(4\text{-tert-butylpyridine})]^+$  (**1**) and  $[\text{Ru}(\text{LH})_2(\text{NCS})(1\text{-methylbenzimidazole})]^+$  (**2**), have efficiencies that are three and two times lower than N719 cells, respectively. Analysis of the UV/Vis and IPCE spectra indicates that the main cause of the reduced efficiencies is a reduced electron collection efficiency ( $\eta_{\text{coll}}$ ). The substituted dyes perform with lower potentials and currents; the impedance is therefore very different for such cells relative to DSCN719 cells when measured at open circuit voltage (open circuit potential) illumination. Furthermore, the lifetime,  $\tau_{\text{eff}}$ , of the electrons in  $\text{TiO}_2$  was reduced by a factor of around ten. This correlated nicely with a reduction in the  $\eta_{\text{coll}}$  values. The low  $\tau_{\text{eff}}$  values may be related to the positive charge on the dyes of **1** and **2**, which results in an enhanced local concentration of  $\text{I}_3^-$  near the photoanode and thereby a higher dark current.

Heated DSCN719 cells result in slightly lower potential, and this alone leads to a change in impedance response when measured at open circuit potential. The same parts of the impedance spectrum are affected when we compare data from heated DSCN719 cells and DSCs prepared with **1** or **2** and not treated thermally (i.e., the interface between photoanode and the electrolyte is affected in the same way).

## Experimental Section

**Chemicals:** The bis(tetrabutylammonium) salt of the complex *cis*-bis(isothiocyanato)bis(2,2'-bipyridyl-4,4'-dicarboxylato)-ruthenium(II), with the trade name Ruthenium 535-bis TBA, referred to as N719 in this paper, was obtained from Solaronix SA (Aubonne, Switzerland). All of the additives were purchased from Sigma–Aldrich and used as received, while the solvents *N,N*-dimethylformamide (DMF) and 3-methoxypropionitrile (3-MPN) were of HPLC grade and obtained from Merck. Ti-Nanoxide HT and Ti-Nanoxide D titan dioxide paste and Pt-Catalyst T/SP were obtained from Solaronix.

**Synthesis of **1** and **2**:** N719 (50 mg) was transferred to a three-necked round-bottomed flask equipped with a condenser and a gas bubbler. The powder was dissolved in DMF (20 mL) that contained either 4-*tert*-butylpyridine or 1-methylbenzimidazole (0.5 M). The solution was deaerated with argon for 1 h and heated at 120 °C under a small flow of argon. After 48 h, water (60 mL) was added, and the diluted solution was eluted through a strong cation exchange column (Varian MEGA-BE-SCX, 1 g, 6 mL) by applying an IST Vac-Master connected to a water suction pump. DMF, the remaining N719, and other impurities were removed by washing with water and methanol. Products **1** or **2** were eluted from the SCX column by an eluent of hydrochloric acid/water/methanol (10:20:70). The SCX eluent was diluted 10 times with water and eluted through a reverse-phase C18 sep-pack column (Varian MEGA-BE-C18, 1 g, 6 mL). The C18 column was carefully washed with a mixture of acetonitrile/water (10:90), and the substitution product was eluted with methanol. The methanol was removed by rotary evaporation, and the product was dried in a vacuum oven at 40 °C.

### Product Analysis by NMR Spectroscopy and LC-MS

The  $^1\text{H}$  NMR spectra were recorded either with a Varian Mercury 300 or a Varian Inova 600 NMR spectrometer at either 300 or 600 MHz. In the 1D spectrum, the digital resolution was 0.25 Hz, and the reference was DMF. The  $^{13}\text{C}$  spectra were recorded with a Varian Mercury 300 instrument at 75 MHz at 25 °C. Typically, 20000 scans were collected. The concentration was 30 mg/mL. The solvent was either  $\text{D}_2\text{O}$  or  $\text{D}_2\text{O}/[\text{D}_6]\text{DMF}$  (1:1). Both solutions were made basic with NaOH to increase the solubility. A 2D HMQC spectrum was also recorded. Correlations to broad  $^1\text{H}$  and  $^{13}\text{C}$  resonances could not be established.

The LC-UV/Vis-ESI-MS equipment and setup used for the product analysis has recently been described.<sup>[17]</sup> The heated capillary temperature of the ESI was set to 200 °C, and the following reject ion mass list for the MS was used:  $m/z = 391, 519, 529, 547, 585, 591, 592$ , and 614.

**Preparation of DSC:** The protocol for the preparation of the DSCs has recently been described.<sup>[15]</sup>

**Photovoltaic Characterization:** A xenon light source was used to give an irradiance of  $100 \text{ W m}^{-2}$ . The spectral output was matched approximately to AM 1.5 conditions by using a water filter. The current–voltage ( $J$ – $V$ ) characteristics of the cell was measured with a digital source meter (Keithley, USA model 2400). The method was to apply an external bias under the given illumination conditions and to measure the generated photocurrent.

**Incident-Photon-to-Current Efficiency (IPCE):** The IPCE measurements were obtained with a home-built IPCE instrument composed of a sample holder and lenses that focus the light from the monochromator (Oriel 77700 MS257). The light intensities were calibrated with a Newport 818-UV/CM detector.

**Electrochemical Impedance Spectroscopy (EIS):** Solar cells were characterized by EIS at open circuit potential created by illumination. The light source used was a 50 W halogen bulb calibrated for a fluence of  $250 \text{ W m}^{-2}$  at the cell surface. A  $3.14 \text{ cm}^2$  circular aperture was placed over the cell to ensure similar illumination conditions during all measurements. Cells were kept at a constant temperature of  $25^\circ\text{C}$  by means of a small calibrated fan. An IM6ex electrochemical workstation from Zahner Elektrik was used to record impedance data at a frequency interval of 1 MHz to 0.01 Hz. The superimposed probe voltage was set at 10 mV in all experiments. The cells were connected in a two-electrode setup with sense and counterelectrode connected to the platinized counterelectrode, and with the work and test electrode connected to the photoelectrode. The main samples were cells that contained either N719, **1**, or **2**. Data were compared to results obtained in a similar fashion but for normal and heated cells containing normal N719 dye.

## Acknowledgments

We thank Prof. Arne Nylandsted Larsen, Physics Department, University of Aarhus, Denmark, for the help with the IPCE measurements and Annette Christensen and Rita Buch for their help with the NMR spectra.

- [1] B. C. O'Regan, M. Grätzel, *Nature* **1991**, 353, 737.
- [2] M. Grätzel, *Inorg. Chem.* **2005**, 44, 6841–51.
- [3] M. Grätzel, *Nature* **2001**, 414, 338–44.
- [4] M. Grätzel, *J. Photochem. Photobiol. C: Photochem. Rev.* **2003**, 4, 145–153.
- [5] A. Hagfeldt, M. Grätzel, *Chem. Rev.* **1995**, 95, 49–68.
- [6] M. Grätzel, *Acc. Chem. Res.* **2009**, 42, 1788–1798.
- [7] A. Hagfeldt, G. Boschloo, H. Lindström, E. Figgemeier, A. Holmberg, V. Aranyos, E. Magnusson, L. Malmqvist, *Coord. Chem. Rev.* **2004**, 248, 1501–1509.
- [8] L. M. Gonçalves, V. Z. Bermudez, H. A. Ribeiro, A. M. Mendes, *Energy Environ. Sci.* **2008**, 1, 655–667.
- [9] J. M. Kroon, N. J. Bakker, H. J. P. Smit, P. Liska, K. R. Thampi, P. Wang, S. M. Zakeeruddin, M. Grätzel, A. Hinsch, S. Hore, U. Würfel, R. Sastrawan, J. R. Durrant, E. Palomares, H. Pettersson, T. Gruszecki, J. Walter, K. Skupien, G. E. Tullloch, *Prog. Photovoltaics. Res. Appl.* **2007**, 15, 1–18.
- [10] M. K. Nazeeruddin, A. Kay, I. Rodicio, R. Humphry-Baker, E. Müller, P. N. Vlachopoulos, M. Grätzel, *J. Am. Chem. Soc.* **1993**, 115, 6382–6390.
- [11] G. Boschloo, L. Häggman, A. Hagfeldt, *J. Phys. Chem. B J. Phys. Chem.* **2006**, 110, 13144.
- [12] H. Kusama, Y. Konishi, H. Sugihara, H. Arakawa, *Sol. Energy Mater. Sol. Cells* **2003**, 80, 167–179.
- [13] H. T. Nguyen, H. M. Ta, T. Lund, *Sol. Energy Mater. Sol. Cells* **2007**, 91, 1934–42.
- [14] P. T. Nguyen, R. Degn, H. T. Nguyen, T. Lund, *Sol. Energy Mater. Sol. Cells* **2009**, 93, 1939–45.
- [15] P. T. Nguyen, A. R. Andersen, E. M. Skou, T. Lund, *Sol. Energy Mater. Sol. Cells* **2010**, 94, 1582–1590.
- [16] I 1215, Crystalline Silicon Terrestrial Photo Voltaic (PV) Modules Design. Qualification and Type Approval, International Electrotechnical commission **1993**.
- [17] F. Nour-Mohammadi, H. T. Nguyen, G. Boschloo, T. Lund, *J. Photochem. Photobiol. A: Chem.* **2007**, 187, 348–55.
- [18] V. Shklover, M.-K. Nazeeruddin, S. M. Sakeeruddin, C. Barbé, a. Kay, T. Haibach, W. Steurer, R. Hermann, H.-U. Nissen, M. Grätzel, *Chem. Mater.* **1997**, 9, 430–439.
- [19] A. K. Banerjee, V. D. Agrawal, R. C. Gupta, *Indian J. Pure Appl. Phys.* **1972**, 10, 538.
- [20] F. Fabregat-Santiago, J. Bisquert, G. Garcia-Belmonte, G. Boschloo, A. Hagfeldt, *Sol. Energy Mater. Sol. Cells* **2005**, 87, 117–131.
- [21] A. R. Andersen, J. Halme, M. I. Ashgar, T. Lund, P. T. Nguyen, Kati Mietunnen, in preparation.
- [22] A referee has suggested that  $\text{I}_3^-$  may interact with the 4-TBP and MBI ligands on **1** and **2**, so sensitized quenching by  $\text{I}_3^-$  may compete with interfacial electron injection, reducing the injection efficiency in cells prepared by **1** and **2** relative to N719 cells.
- [23] M. J. Frisch, G. W. Trucks, H. B. Schlegel, G. E. Scuseria, M. A. Robb, J. R. Cheeseman, G. Scalmani, V. Barone, B. Mennucci, G. A. Petersson, H. Nakatsuji, M. Caricato, X. Li, H. P. Hratchian, A. F. Izmaylov, J. Bloino, G. Zheng, J. L. Sonnenberg, M. Hada, M. Ehara, K. Toyota, R. Fukuda, J. Hasegawa, M. Ishida, T. Nakajima, Y. Honda, O. Kitao, H. Nakai, T. Vreven, J. A. Montgomery Jr., J. E. Peralta, F. Ogliaro, M. Bearpark, J. J. Heyd, E. Brothers, K. N. Kudin, V. N. Staroverov, R. Kobayashi, J. Normand, K. Raghavachari, A. Rendell, J. C. Burant, S. S. Iyengar, J. Tomasi, M. Cossi, N. Rega, J. M. Millam, M. Klene, J. E. Knox, J. B. Cross, V. Bakken, C. Adamo, J. Jaramillo, R. Gomperts, R. E. Stratmann, O. Yazyev, A. J. Austin, R. Cammi, C. Pomelli, J. W. Ochterski, R. L. Martin, K. Morokuma, V. G. Zakrzewski, G. A. Voth, P. Salvador, J. J. Dannenberg, S. Dapprich, A. D. Daniels, O. Farkas, J. B. Foresman, J. V. Ortiz, J. Cioslowski, D. J. Fox, *Gaussian 09*, Revision A.02, Gaussian, Inc., Wallingford, CT, **2009**.

Received: September 1, 2010  
Published Online: April 26, 2011